Chinese Chemical Letters 34 (2023) 107532

Contents lists available at ScienceDirect

Chinese Chemical Letters

journal homepage: www.elsevier.com/locate/cclet

Blue-shifted and naked-eye recognition of $H_2PO_4^-$ and acetylacetone based on a luminescent metal–organic framework with new topology and good stability

Shuli Yao[a], Hui Xu[a], Tengfei Zheng[a], Yunwu Li[c], Haiping Huang[a], Jun Wang[b], Jinglin Chen[a], Suijun Liu[a,b,*], Herui Wen[a,*]

[a] School of Chemistry and Chemical Engineering, Jiangxi Provincial Key Laboratory of Functional Molecular Materials Chemistry, Jiangxi University of Science and Technology, Ganzhou 341000, China
[b] Fujian Key Laboratory of Functional Marine Sensing Materials, Minjiang University, Fuzhou 350108, China
[c] Shandong Provincial Key Laboratory of Chemical Energy Storage and Novel Cell Technology, School of Chemistry and Chemical Engineering, Liaocheng University, Liaocheng 252000, China

ARTICLE INFO

Article history:
Received 17 March 2022
Revised 8 May 2022
Accepted 13 May 2022
Available online 17 May 2022

Keywords:
Metal-organic framework
Fluorescence sensing
Naked-eye recognition
Fluorescence blue shift
$H_2PO_4^-$ and acetylacetone

ABSTRACT

Fluorescence detecting both organic and inorganic analytes has aroused tremendous scientific interests, because fluorescence techniques have high sensitivity and are easy to operate. A new three-dimensional (3D) MOF $\{[(CH_3)_2NH_2][Zn_3(bbip)(BTDI)_{1.5}(OH)]\cdot DMF\cdot MeOH\cdot 3H_2O\}_n$ (**JXUST-13**, bbip = 2,6-bis(benzimidazol-1-yl)pyridine and H_4BTDI = 5,5′-(benzo[*c*][1,2,5]thiadiazole-4,7-diyl)diisophthalic acid) with new 4,4,8-connceted topology has been successfully synthesized and structurally characterized. Importantly, **JXUST-13** could recognize $H_2PO_4^-$ and acetylacetone (Acac) by obvious fluorescence blue shift and slight enhancement with the detection limits of 2.70 μmol/L and 0.21 mmol/L, respectively. In addition, **JXUST-13** exhibits relatively good thermal stability, chemical stabilities as well as reusability, and the analytes could be distinguished by naked eye and fluorescence test paper. Remarkably, **JXUST-13** is the first dual-responsive MOF sensor based on fluorescence blue shift for the detection of $H_2PO_4^-$ and Acac with good selectivity in a handy, economic, and environmentally friendly manner.

With environmental pollution being more and more serious, the detection of toxic contaminants including organic and inorganic substances becomes a hot research field. In recent years, fluorescence sensors for detecting analytes have aroused tremendous scientific interests, because fluorescence techniques have high sensitivity and are easy to operate. Metal-organic frameworks (MOFs) with unique structures advantages and diverse properties, such as chemical sensors [1], catalysis [2], gas adsorption and separation [3,4], drug delivery [5], conduction [6,7], have become star materials in materials and chemistry. Many MOFs are reasonably designed [8,9]. In addition, MOFs as fluorescence sensors, possess the advantages of good selectivity, high sensitivity, short response time and low cost, *etc.* [1], which were widely applied in detecting anions [10], volatile organic compounds [11], explosives [12], cations and antibiotics [13,14], organic molecules [15,16], *etc.* Three effects are displayed in the MOF fluorescence sensing, including fluorescence quenching (turn-off effect), fluorescence enhancement (turn-on effect) and fluorescence shift. Compared to turn-off effect, turn-on effect has higher sensitivity and is easier to identify; fluorescence shift has a noticeable color change, which could clearly distinguish target analytes with other substances. Therefore, exploring shifted and turn-on MOFs sensor is significant and meaning.

Both inorganic phosphates (mainly PO_4^{3-}, HPO_4^{2-} and $H_2PO_4^-$) and organic molecule acetylacetone (Acac) are toxic. Phosphates are essential nutritional ingredients during the growth of the organism, and play important roles in building energy carriers, nucleic acids and proteins in biological systems [17]. The high levels of phosphates have a direct correlation to cardiovascular disease and kidney failure, and the low levels of phosphates could cause hypophosphatemia in biological liquids [18]. In addition, high concentration of phosphates released in aquatic ecosystems could cause serious environmental problems, such as eutrophication and overgrowth of algae in aquatic systems [19]. Therefore, it is highly essential to detect inorganic phosphates. As for Acac, it is extensively used in industry, including modifier, chelating agents, inter-

* Corresponding authors at: School of Chemistry and Chemical Engineering, Jiangxi Provincial Key Laboratory of Functional Molecular Materials Chemistry, Jiangxi University of Science and Technology, Ganzhou 341000, China.
E-mail addresses: sjliu@jxust.edu.cn (S. Liu), wenherui63@163.com (H. Wen).

https://doi.org/10.1016/j.cclet.2022.05.046
1001-8417/

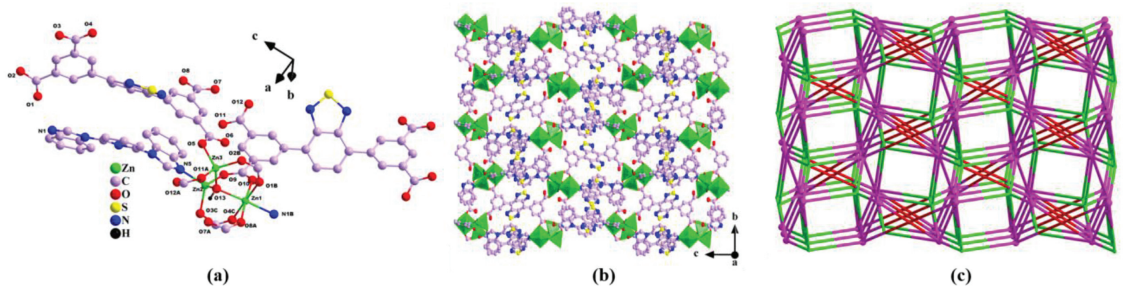

Fig. 1. (a) The coordination environment of Zn^{II} ions in **JXUST-13** (H atoms omitted for clarity except μ_3-OH), symmetry codes: A: -*x*+1/2, *y*+1/2, -*z*+1/2; B: *x* - 1/2, -*y*+3/2, *z* - 1/2; C: *x*+1/2, -*y*+3/2, *z* - 1/2. (b) The 3D structure of **JXUST-13**. (c) Topological structure of **JXUST-13**.

mediate, precursor, additive *etc.* [20]. Due to the toxicity, volatility and flammability, Acac exposed to the air could cause environmental pollution and health problems, such as nausea, headache and vomiting upon inhalation [20]. Thus, it is urgent to develop advanced materials for rapidly and sensitively recognizing Acac.

Compared with other analytical techniques, MOFs-based fluorescence recognition has become more popular due to the significant advantages, and large numbers of MOF-based fluorescence sensors for various analytes have been reported. To date, many MOF sensors for PO_4^{3-} have been reported [21–25], while only four MOF-based fluorescence sensors for $H_2PO_4^-$ were investigated with turn-off effect or post-synthetic modification [26–29], and the blue-shifted sensor toward $H_2PO_4^-$ is just one [28]. In addition, a large number of MOF sensors for Acac were studied in recent years [30–37]. However, most of them displayed turn-off effect, and only three turn-on [32,35,36] and one red-shifted [37] MOF sensors were explored. Blue-shifted MOF sensor toward Acac has never been reported. Thence, it is worthy and meaningful to develop dual functional fluorescence blue-shifted MOF sensor for detecting of $H_2PO_4^-$ and Acac.

Given these background and knowledge, luminescent MOF was rationally designed and constructed by Zn^{II} ion, basic bis(benzimidazol)pyridine and acidic benzothiadiazole-functionalized ligands. Bis(benzimidazol)pyridine ligand has potential uncoordinated active site, which is beneficial to interact with analyte. Benzothiadiazole derivatives with π-conjugated and electron-deficient group, which possess excellent visible optical and electronic properties [38], are good candidates for fluorescent material. It should be noted that Zn^{II}-based MOFs for detecting analytes are based on ligand-centered luminescence [27]. However, ligand-center-based luminescence sensors have small Stokes shifts, and the color difference between the excitation and emission light is not obvious, which prevents the naked eye recognition of analytes [27]. Herein, a novel luminescent MOF $\{[(CH_3)_2NH_2][Zn_3(bbip)(BTDI)_{1.5}(OH)]\cdot DMF\cdot MeOH\cdot 3H_2O\}_n$ (**JXUST-13**) with 3D new topology was successfully synthesized by 5,5′-(benzo[*c*][1,2,5]thiadiazole-4,7-diyl)diisophthalic acid (H_4BTDI) and 2,6-bis(benzimidazol-1-yl)pyridine (bbip) ligands (Scheme S1 in Supporting information). Importantly, **JXUST-13** could successfully sense $H_2PO_4^-$ and Acac *via* fluorescence blue shift and naked eye. To the best of our knowledge, **JXUST-13** is the first dual-responsive MOF sensor toward $H_2PO_4^-$ and Acac based on fluorescence blue shift.

Single-crystal X-ray diffraction analysis reveals that **JXUST-13** crystallizes in monoclinic system $P2_1/n$ space group and takes a 3D framework (Table S1 in Supporting information). The asymmetric unit includes three crystallographically independent Zn^{II} ions, one bbip ligand, one and a half $BTDI^{4-}$ ligands, one μ_3-OH, one $(CH_3)_2NH_2^+$ cation, one DMF, one MeOH and three H_2O molecules. As shown in Fig. 1a, Zn1 ion displays a six-coordinated environment constructed by one N atom (N1B) from one bbip ligand and five O atoms (O1B, O4C, O8A, O10 and O13) from four $BTDI^{4-}$ ligands and one μ_3-OH. Zn2 ion exhibits a four-coordinated environment building with three O atoms (O3C, O9 and O13) from two $BTDI^{4-}$ ligands and one μ_3-OH, and one N atom (N5) from one bbip ligand; Zn3 ion behaves a four-coordinated environment with four O atoms (O2B, O5, O11A and O13) from three $BTDI^{4-}$ ligands and one μ_3-OH. The coordination geometries of Zn^{II} ions could be viewed as octahedron, tetrahedron and tetrahedron, respectively, calculated by SHAPE 2.1 software (Table S3 in Supporting information) [39]. Moreover, the adjacent Zn^{II} ions constitute a $[Zn_3(\mu_3\text{-}OH)(COO)_3]$ secondary building unit (SBU), which constructed by one μ_3-OH and three bridging carboxylates. The distances of Zn-O and Zn-N bonds are in the range of 1.948(3)–2.141(4) Å and 2.002(4)–2.140(4) Å, respectively (Table S2 in Supporting information). Furthermore, the SBUs are linked by $BTDI^{4-}$ ligands to build a two-dimensional (2D) layer structure (Fig. S1 in Supporting information). The 2D layers are further connected by bbip and $BTDI^{4-}$ ligands to conform a 3D framework (Fig. 1b). Interestingly, the $BTDI^{4-}$ ligands display two different coordination fashions in **JXUST-13** (Fig. S2 in Supporting information). The topological analysis indicates that **JXUST-13** takes a new 4,4,8-connceted topology with Schlafli symbol $\{3.4^3.5^2\}_2\{3^2.4^2.5^2\}\{3^4.4^6.5^8.6^{10}\}_2$ rationalized by TOPOS 4.0 [40]. Among them, the $BTDI^{4-}$ ligand is considered as a 4-connected node, and the $[Zn_3(\mu_3\text{-}OH)(COO)_3]$ SBU is viewed as a 8-connected node (Fig. 1c). The total solvent-accessible volume of **JXUST-13** is 2048.0 $Å^3$ and the porosity is 30.3% per unit cell without solvent molecules, which is estimated by PLATON [41]. In addition, the porous property of **JXUST-13** also was carried out by N_2 adsorption−desorption isotherm experiment. As displayed in Fig. S3 (Supporting information), type I adsorption isotherm is obtained, and the calculated BET surface area is 371.2 m^2/g, which verify the existence of microporous pores in **JXUST-13**.

The chemical stabilities in organic solvents, neutral H_2O, acid-base aqueous solutions were also determined by PXRD patterns. The peak positions of PXRD patterns of **JXUST-13** soaked in pyridine, *n*-hexane, acetonitrile, tetrahydrofuran (THF), methanol (MeOH), dimethyl sulfoxide (DMSO), *N*,*N*-dimethylacetamide (DMA), *N*,*N*-dimethylformamide (DMF), CH_2Cl_2, acetone and Acac for 24 h basically unchanged, revealing the framework still retains and **JXUST-13** displays good solvent stability (Fig. 2a). Besides, NaOH and HCl were used to prepare aqueous solution with different pH values. The samples were soaked in the aqueous solution with pH values scope from 2 to 12 for 12 h, and PXRD patterns remained unchanged (Fig. 2b), indicating relatively good acid-base stability of **JXUST-13**.

MOFs constructed by metal centers with d^{10} electronic configuration and conjugated organic ligands are potential fluorescence sensing material [30]. Therefore, **JXUST-13** was explored the fluorescence sensing properties toward analytes. The solid emission spectra were measured at room temperature. As shown in Fig. S4 (Supporting information), the emission peaks of H_4BTDI and bbip

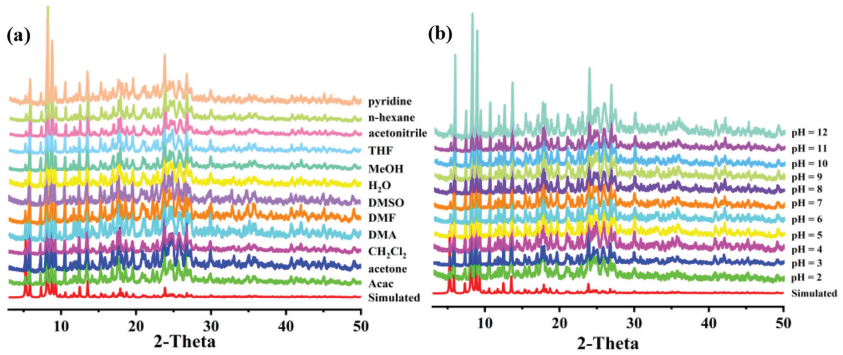

Fig. 2. (a) PXRD patterns of **JXUST-13** immersed in H_2O and some common organic solvents for 24 h. (b) PXRD patterns of **JXUST-13** soaked in different aqueous solutions with pH values from 2 to 12 for 12 h.

are observed at 515 nm ($\lambda_{ex} = 370$ nm) and 374 nm ($\lambda_{ex} = 330$ nm), respectively, which could be ascribed to the $\pi^* \rightarrow \pi$ or $\pi^* \rightarrow$ n electron transition within the ligands [34]. While, the emission band of **JXUST-13** appears at 493 nm ($\lambda_{ex} = 370$ nm), which may stem from the metal-perturbed intraligand charge transfer because of the d^{10} electron configuration of Zn^{II}. Compared with H_4BTDI ligand, the emission band of **JXUST-13** displays an obvious blue shift resulted from coordination interactions between metal ions and organic ligands [35].

Due to the environmentally friendly characteristic, similar emission band with solid state (Fig. S5a in Supporting information), as well as good stability in EtOH solution, EtOH was chosen as dispersant to explore the sensing behavior of **JXUST-13**. **JXUST-13** was fully grinded and added to EtOH solution with the concentration of 0.25 mg/mL. After ultrasonic treatment for 30 min, a stable suspension was obtained. 5 μL Different anions aqueous solution (including ACO^-, NO_3^-, Br^-, Cl^-, F^-, I^-, CO_3^{2-}, SO_4^{2-}, WO_4^{2-}, HCO_3^-, PO_4^{3-}, HPO_4^{2-} and $H_2PO_4^-$, 0.2 mol/L, potassium or sodium salt, and the cations almost have no influence on the emission, Fig. S5b in Supporting information) were added to 2 mL EtOH suspension in 3 mL quartz cuvette for testing. As illustrated in Fig. 3a, the fluorescence performances have important relationship with anions type. Most of anions did not occur significant fluorescence changes, while $H_2PO_4^-$ displayed an obvious fluorescence blue shift and slight enhancement, which could be distinguished by naked eye under 365 nm portable UV lamp (Fig. 3a, illustration). The color change from green to blue also is confirmed by CIE chromaticity diagram (Fig. 3b). The result revealed that **JXUST-13** displayed good selectivity toward $H_2PO_4^-$ by fluorescence blue shift. The anti-interference experiment also was performed with 5 μL $H_2PO_4^-$ and the same concentration of other anions into EtOH suspensions, and the fluorescence blue shift still exists (Fig. S6a in Supporting information), implying the remarkable sensitivity of **JXUST-13** toward $H_2PO_4^-$.

Moreover, the fluorescence titration experiments were carried out with increasing $H_2PO_4^-$ concentration (0.02 mol/L). As manifested at Fig. 3c (illustration), the fluorescence change with blue shift and enhancement by the increasing of $H_2PO_4^-$ concentration. A good linear correlation of fluorescence intensity ratios I/I_0 and concentration with $R^2 = 0.998$ was obtained (Fig. 3d). The detection limit was 2.70 μmol/L calculated by the formula of $3\sigma/k$ (σ: the standard error; k: the slope). These results indicated that **JXUST-13** could be viewed as a fluorescence blue-shift sensor toward $H_2PO_4^-$ with high sensitivity and selectivity.

The possible sensing mechanism of **JXUST-13** toward $H_2PO_4^-$ was discussed. The peak positions of PXRD patterns about **JXUST-13** immersed in EtOH and $H_2PO_4^-$ solution for 24 h remained unchanged (Fig. S8c in Supporting information), indicating that basic framework remained intact after reacting with $H_2PO_4^-$, thus, it excluded the impact of skeleton collapse. The IR spectrum of **JXUST-13** incubated with $H_2PO_4^-$ and EtOH showed no obvious peak positions shift compared with **JXUST-13** (Fig. S10 in Supporting information), demonstrating that there are no coordination or hydrogen bonding interactions between $H_2PO_4^-$ and **JXUST-13**. The XPS results also indicated that there was no coordination interaction due to the similar binding energy of Zn 2p (Fig. S11a in Supporting information). Besides, the XPS spectra of O 1s, N 1s and S 2p also demonstrated that there was no interaction between $H_2PO_4^-$ and O/N/S atoms, which were consistent with IR spectra. In addition, $H_2PO_4^-$ could well disperse in suspension and attach on MOF particles surface, leading to host-guest interactions. The UV−vis absorption spectra of **JXUST-13** suspension adding with different anions were characterized. There was an obvious absorption spectral change of $H_2PO_4^-$ ion in **JXUST-13** suspension, indicating the possible existence of interaction between $H_2PO_4^-$ and MOF (Fig. S12a in Supporting information). The average fluorescence lifetime (τ_{av}) of **JXUST-13**@$H_2PO_4^-$ (6.12×10^{-3} ms) was shorter than that of **JXUST-13** (1.02×10^{-2} ms) (Figs. S13a and b in Supporting information), further revealing the occurrence of excited state interaction between $H_2PO_4^-$ and **JXUST-13** [31]. In general, when the excited electrons transferred from a high-lying π^*-type lowest unoccupied molecular orbital (LUMO) to the conduction band (CB) of MOF, fluorescence enhancement could emerge [42]. As shown in Fig. S14 (Supporting information), there was no overlap between absorption spectrum of $H_2PO_4^-$ and the emission spectrum of MOF, therefore, fluorescence resonance energy transfer (FRET) is not the mechanism of the observed fluorescence enhancement. Moreover, the observed fluorescence blue shift may indicate the formation of strong exciplex between **JXUST-13** and $H_2PO_4^-$ [43]. Exciplex is an excited complex, which generally formed through the interaction of an excited molecule with an unexcited molecule. Therefore, the obvious fluorescence blue shift and slight enhancement of **JXUST-13** toward $H_2PO_4^-$ may be due to the formation of exciplex and charge transfer between $H_2PO_4^-$ and framework.

The same method of anions sensing was used to prepare EtOH suspension of **JXUST-13**. The fluorescence sensing performances toward common small organic molecules also were explored. 5 μL different organic molecules including DMF, DMA, 1-propanol, ethylene glycol, pyridine, *n*-hexane, acetonitrile, THF, MeOH, DMSO, CH_2Cl_2, acetone, formaldehyde and Acac were added to 2 mL EtOH suspension and tested in 3 mL quartz cuvette. As exhibited in Fig. 4a, fluorescence behaviors were relevant to the type of organic molecules. Among them, Acac manifested obvious fluorescence blue shift and slight enhancement, and other of them had weak influence on the emission. In addition, the fluorescence blue shift could be easily identified by naked eye under 365 nm portable UV lamp (Fig. 4a, illustration) and the CIE chromaticity diagram (Fig. 4b). These results indicated that **JXUST-13** had good selec-

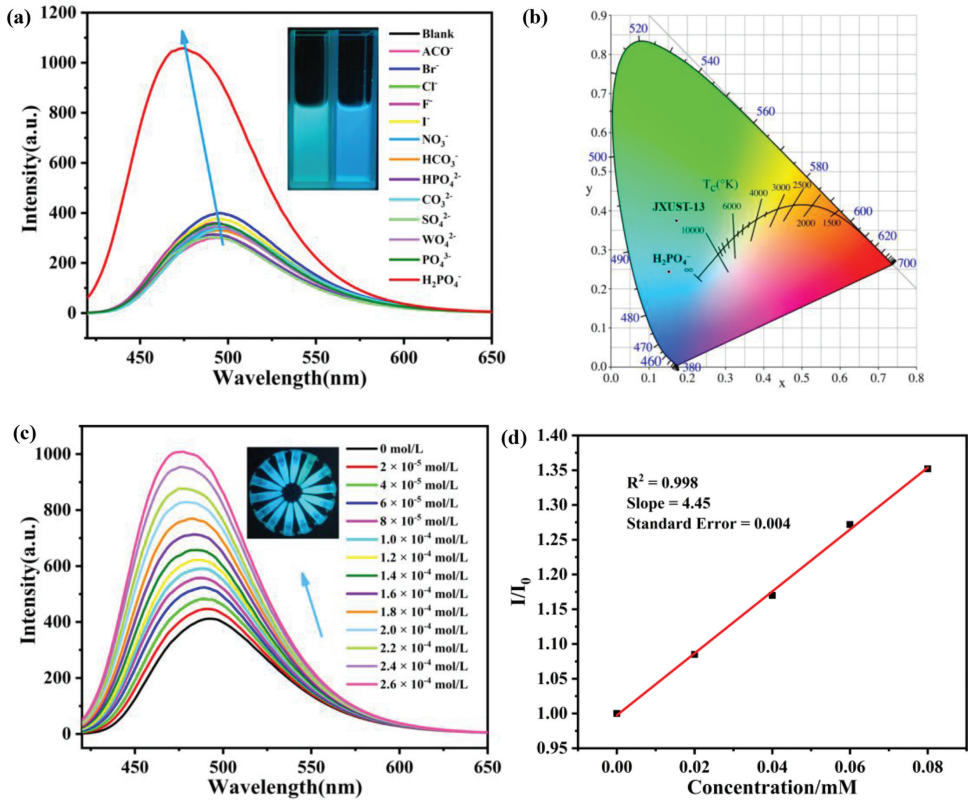

Fig. 3. (a) Emission spectra of **JXUST-13** in EtOH suspension with 5 μL 0.2 mol/L different anions (λ_{ex} = 370 nm), inset: naked eye recognition image of blank (left) and **JXUST-13**@$H_2PO_4^-$ (right) under 365 nm portable UV lamp. (b) The CIE chromaticity diagram of **JXUST-13** and **JXUST-13** added with $H_2PO_4^-$ in EtOH suspension. (c) Emission spectra of **JXUST-13** with different concentrations of $H_2PO_4^-$ (illustration). (d) The correlation between fluorescence intensity ratio I/I_0 and the concentration of $H_2PO_4^-$.

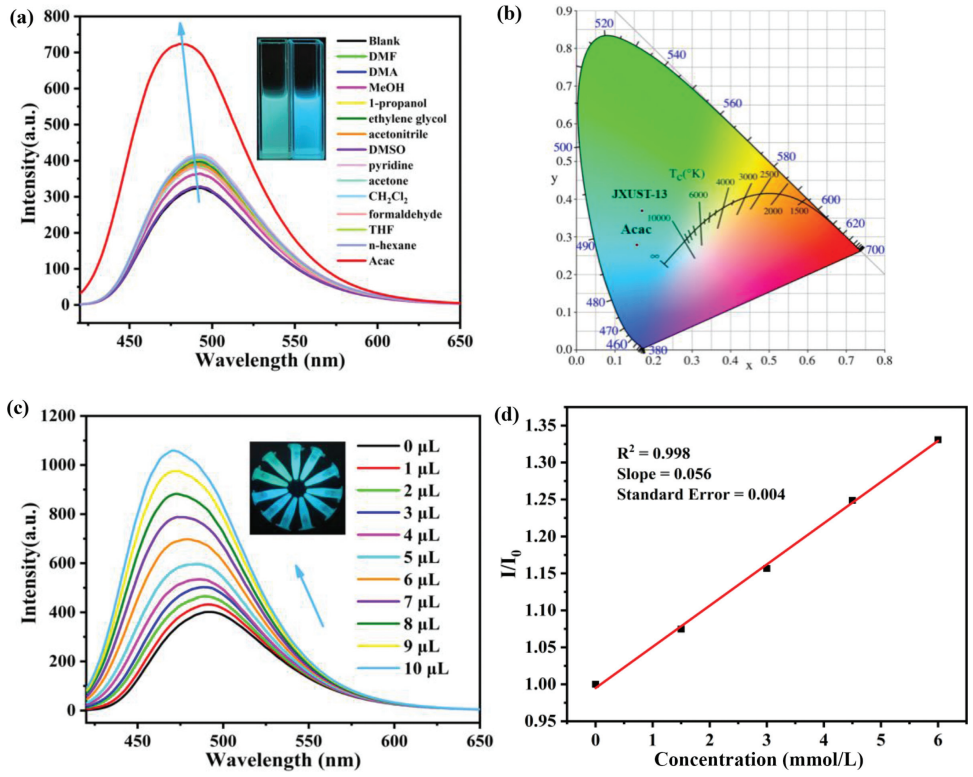

Fig. 4. (a) Emission spectra of **JXUST-13** with 5 μL different organic molecules in EtOH suspension (λ_{ex} = 370 nm), inset: naked eye recognition images of blank (left) and **JXUST-13**@Acac (right) under 365 nm portable UV lamp. (b) The CIE chromaticity diagram of **JXUST-13** and **JXUST-13** with Acac in EtOH suspension. (c) Emission spectra of **JXUST-13** with different concentrations of Acac (illustration). (d) The correlation between fluorescence intensity ratio I/I_0 and the concentration of Acac.

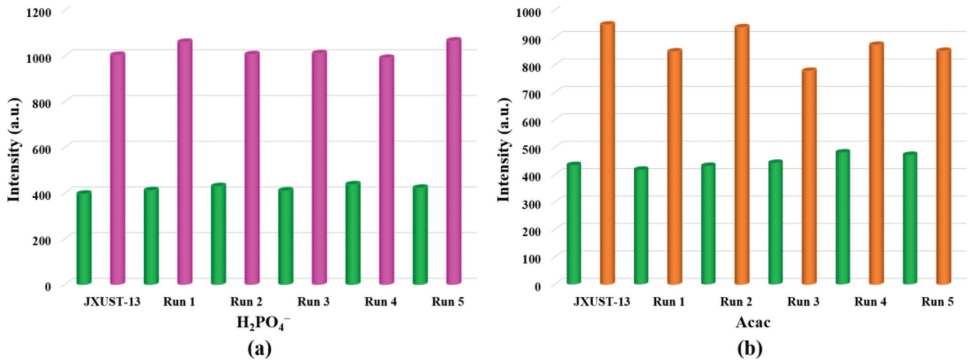

Fig. 5. Fluorescence intensities of **JXUST-13** after five times of recycling for (a) $H_2PO_4^-$ and (b) Acac ($\lambda_{ex} = 370$ nm). The green pillars represent the blank of EtOH suspension, and the pink or orange pillars show the suspension after adding of $H_2PO_4^-$ or Acac.

tivity for Acac by fluorescence blue shift. Furthermore, the anti-interference experiment also was performed. 5 μL other organic molecules with Acac were added into EtOH suspensions, and the fluorescence blue shift still exists (Fig. S6b in Supporting information), further confirming that **JXUST-13** had excellent sensitivity toward Acac by fluorescence blue shift.

In order to explore the fluorescence performance of **JXUST-13** with different concentration of Acac, the titration experiment was carried out with Acac diluted to 30% (v/v). The fluorescence showed blue shift and enhancement with the increasing of Acac concentration (Fig. 4c, illustration). Besides, the correlation between fluorescence intensity ratio I/I_0 and concentration was also measured at low concentration range, which revealed a good linear correlation with $R^2 = 0.998$ (Fig. 4d). The detection limit was 0.21 mmol/L calculated by $3\sigma/k$. These results indicated that **JXUST-13** can be considered as a potential sensor for Acac by fluorescence blue shift with good sensitivity and selectivity.

The possible sensing mechanism of **JXUST-13** toward Acac was elucidated. The PXRD pattern indicated that framework of **JXUST-13** kept intact after detecting Acac (Fig. S8c in Supporting information). Acac can be well dispersed in suspension, and host-guest interaction is easy to occur. The UV−vis absorption spectra demonstrated the possible presence of interaction between Acac and **JXUST-13**, due to the obvious change of absorption spectrum after adding Acac into **JXUST-13** suspension (Fig. S12b in Supporting information). Moreover, the average fluorescence lifetime (τ_{av}) further proved the excited state interaction between **JXUST-13** and Acac, because the lifetime of **JXUST-13**@Acac (6.13×10^{-3} ms) was shorter than that of **JXUST-13** (1.02×10^{-2} ms) (Figs. S13a and c in Supporting information) [31,44]. It is well known that Acac has keto−enol tautomerism, which might introduce H-bonding interaction between the -OH moiety of enol form of Acac and the oxygen atoms of ligand [30]. The IR spectrum about **JXUST-13** incubated with Acac and EtOH showed that there was a peak position shift from 1373 cm^{-1} (**JXUST-13**) to 1381 cm^{-1} (**JXUST-13**@Acac), corresponding to the symmetric stretching of $-COO^-$ [21], which might manifest the formation of hydrogen bond interaction between **JXUST-13** and Acac (Fig. S10 in Supporting information). In addition, due to the d^{10} electronic configuration of Zn^{II}, the fluorescence of Zn-MOFs mostly stems from the intraligand charge transfer. In general, the excited electrons transfer from a high-lying π^*-type LUMO to the CB of MOFs, fluorescence enhancement could occur [42,45]. While FRET is not the possible mechanism of fluorescence enhancement, owing to no overlap between absorption spectrum of Acac and the emission spectrum of **JXUST-13** (Fig. S14 in Supporting information). Moreover, the observed fluorescence blue shift may be the formation of exciplex between MOF and Acac [42,43]. Therefore, the possible sensing mechanisms of fluorescence blue shift and slight enhancement toward Acac were the existence of H-bonding interaction, the formation of exciplex and charge transfer between Acac and **JXUST-13**.

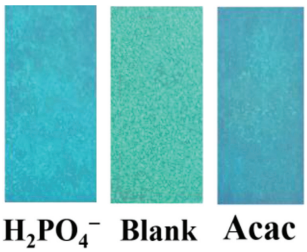

Fig. 6. The fluorescence test papers of **JXUST-13** and **JXUST-13** with $H_2PO_4^-$ and Acac under 365 nm UV portable lamp.

Reusability also was an important index in practical applications. Thus, a quick and easy way of cycleability toward $H_2PO_4^-$ and Acac was performed. The as-synthesized sample of **JXUST-13** was soaked in 2 mL EtOH and 5 μL $H_2PO_4^-$/Acac solutions for 20 min. After washing by ethanol five runs and drying in the air, the samples were characterized with emission spectra and PXRD patterns. The fluorescence enhancement and blue shift behavior still retained (Figs. 5a and b). The PXRD patterns of **JXUST-13** after five times cycle matched well with the simulated one (Fig. S8d in Supporting information), revealing the good stability of framework during the cyclic process. Thence, **JXUST-13** could be recycled at least five times for $H_2PO_4^-$ and Acac sensing.

In addition, fluorescent test paper was a fast and portable method to detect analytes. The filter papers with suitable size were immersed in EtOH suspension and air dried. Then the test papers were putted into $H_2PO_4^-$ or Acac solution, respectively. Importantly, blue lights were discovered on the fluorescent test papers under excited at 365 nm UV portable lamp (Fig. 6), which revealed that **JXUST-13** could fastly detect $H_2PO_4^-$ and Acac with a test paper.

In summary, a new 3D Zn^{II}-based MOF (**JXUST-13**) with new 4,4,8-connceted topology has been successfully designed and synthesized by mixed-ligands strategy. Importantly, **JXUST-13** could detect $H_2PO_4^-$ and Acac by obvious fluorescence blue shift and slight enhancement in EtOH suspension. The sensing mechanism of $H_2PO_4^-$ may be ascribed to the formation of exciplex and charge transfer between $H_2PO_4^-$ and **JXUST-13**. And the sensing mechanism for Acac may be attributed to hydrogen bonding interactions, the formation of exciplex and charge transfer between Acac and **JXUST-13**. In addition, it could also be quickly and conveniently recognized by naked eye and fluorescence test papers. To our best knowledge, **JXUST-13** could act as the first dual-responsive MOF sensor based on fluorescent blue shift and naked-eye detecting of

$H_2PO_4^-$ and Acac. Further researches of MOF fluorescence probes are underway in our lab.

Declaration of competing interest

The authors declare no competing financial interest.

Acknowledgments

This work was supported by the National Natural Science Foundation of China (Nos. 22061019, 21861018, 22161019 and 12174172), the NSF of Jiangxi Province (No. 20202ACBL213001), Jiangxi Provincial Key Laboratory of Functional Molecular Materials Chemistry (No. 20212BCD42018), Fujian Key Laboratory of Functional Marine Sensing Materials, Minjiang University (No. MJUKF-FMSM202010), the Youth Jinggang Scholars Program in Jiangxi Province (No. QNJG2019053), the Two Thousand Program in Jiangxi Province (No. jxsq2019201068) and the Special Foundation for Postgraduate Innovation in Jiangxi Province (No. YC2020-B155).

Supplementary materials

Supplementary material associated with this article can be found, in the online version, at doi:10.1016/j.cclet.2022.05.046.

References

[1] D. Tian, X.J. Liu, R. Feng, et al., ACS Appl. Mater. Interfaces 10 (2018) 5618–5625.
[2] Y. Yan, R. Abazari, J. Yao, J. Gao, Dalton Trans. 50 (2021) 2342–2349.
[3] H. Li, K. Wang, Y. Sun, et al., Mater. Today 21 (2018) 108–121.
[4] G. Si, X. Kong, T. He, et al., Chin. Chem. Lett. 32 (2021) 918–922.
[5] X. Liu, T. Liang, R. Zhang, et al., ACS Appl. Mater. Interfaces 13 (2021) 9643–9655.
[6] X.N. Zou, D. Zhang, Y. Xie, et al., Inorg. Chem. 60 (2021) 10089–10094.
[7] A.A. Zhang, X. Cheng, X. He, et al., Research 2021 (2021) 9874273.
[8] B. Wang, H. Yang, Y.B. Xie, et al., Chin. Chem. Lett. 27 (2016) 502–506.
[9] J. Sun, X. Zhang, D. Zhang, et al., CCS Chem. 4 (2022) 996–1006.
[10] K. Xing, R.Q. Fan, X.Y. Liu, et al., Chem. Commun. 56 (2020) 631–634.
[11] H.Y. Li, S.N. Zhao, S.Q. Zang, J. Li, Chem. Soc. Rev. 49 (2020) 6364–6401.
[12] Z.J. Qiu, S.T. Fan, C.Y. Xing, et al., ACS Appl. Mater. Interfaces 12 (2020) 55299–55307.
[13] L. Fan, D. Zhao, B. Li, et al., Spectrochim. Acta A 264 (2022) 120232.
[14] B. Wang, X.L. Lv, D. Feng, et al., J. Am. Chem. Soc. 138 (2016) 6204–6216.
[15] S.L. Yao, H. Xu, T.F. Zheng, et al., Cryst. Growth Des. 21 (2021) 5765–5772.
[16] B. Wang, P. Wang, L.H. Xie, et al., Nat. Commun. 10 (2019) 3861.
[17] X. Song, Y. Ma, X. Ge, et al., RSC Adv. 7 (2017) 8661–8669.
[18] S.Z. Du, Z. Sun, L. Han, et al., Sens. Actuators B: Chem. 324 (2020) 128757.
[19] Z. Li, G. Liu, C. Fan, S. Pu, Anal. Bioanal. Chem. 413 (2021) 3281–3290.
[20] Y. Li, J.D. An, T.T. Wang, et al., Dye. Pigment. 186 (2021) 109039.
[21] K. Yi, X. Zhang, L. Zhang, Sci. Total Environ. 772 (2021) 144952.
[22] M. Chen, K.Y. Wu, W.L. Pan, et al., Spectrochim. Acta A 247 (2021) 119084.
[23] B. Qin, X. Zhang, J. Zhang, Cryst. Growth Des. 20 (2020) 5120–5128.
[24] H. Xu, C.S. Cao, B. Zhao, Chem. Commun. 51 (2015) 10280–10283.
[25] J. Yang, Y. Dai, X. Zhu, et al., J. Mater. Chem. A 3 (2015) 7445–7452.
[26] K. Naskar, A.K. Bhanja, S. Paul, K. Pal, C. Sinha, Cryst. Growth Des. 20 (2020) 6453–6460.
[27] D.K. Singha, P. Majee, S. Hui, S.K. Mondal, P. Mahata, Dalton Trans. 49 (2020) 829–840.
[28] R. Dalapati, S. Biswas, Sens. Actuators B: Chem. 239 (2017) 759–767.
[29] K.S. Asha, R. Bhattacharjee, S. Mandal, Angew. Chem. Int. Ed. 55 (2016) 11528–11532.
[30] G. Chakraborty, P. Das, S.K. Mandal, ACS Appl. Mater. Interfaces 12 (2020) 11724–11736.
[31] M.M. Fu, L. Fu, G.H. Cui, Dalton Trans. 50 (2021) 10180–10186.
[32] S. Ghosh, A. Das, S. Biswas, Microporous Mesoporous Mat. 323 (2021) 111251.
[33] X.M. Kang, X.Y. Fan, P.Y. Hao, W.M. Wang, B. Zhao, Inorg. Chem. Front. 6 (2019) 271–277.
[34] J.Y. Zou, L. Li, S.Y. You, et al., Cryst. Growth Des. 18 (2018) 3997–4003.
[35] S.L. Yao, S.J. Liu, X.M. Tian, et al., Inorg. Chem. 58 (2019) 3578–3581.
[36] Y. Yu, Y. Wang, H. Xu, et al., CrystEngComm 22 (2020) 3759–3767.
[37] L.Q. Li, S.L. Yao, X.M. Tian, et al., CrystEngComm 23 (2021) 2532–2537.
[38] X. Han, Z. Wang, Q. Cheng, et al., Dye. Pigment. 145 (2017) 576–583.
[39] M. Llunell, D. Casanova, J. Cirera, P. Alemany, S. Alvarez, SHAPE, Version 2.1, Universitat de Barcelona, 2013.
[40] V.A. Blatov, A.P. Shevchenko, TOPOS, Version 4.0 Professional (Beta Evaluation), Samara State University, 2006.
[41] A.L. Spek, Acta Cryst. C71 (2015) 9–18.
[42] F. Wang, C. Dong, Z. Wang, et al., Eur. J. Inorg. Chem. 2014 (2014) 6239–6245.
[43] S. Pramanik, Z. Hu, X. Zhang, et al., Chem. Eur. J. 19 (2013) 15964–15971.
[44] Q.Q. Xiao, G.Y. Dong, Y.H. Li, G.H. Cui, Inorg. Chem. 58 (2019) 15696–15699.
[45] S. Pramanik, C. Zheng, X. Zhang, T.J. Emge, J. Li, J. Am. Chem. Soc. 133 (2011) 4153–4155.